Inorganic Chemistry

Article

pubs.acs.org/IC

Is $BiPO_4$ a Better Luminescent Host? Case Study on Doping and Annealing Effects

Minglei Zhao,[†] Liping Li,[‡] Jing Zheng,[‡] Liusai Yang,[‡] and Guangshe Li*[,†]

[†]State Key Laboratory of Structural Chemistry, Fujian Institute of Research on the Structure of Matter, Graduate School of Chinese Academy of Sciences, Fuzhou 350002, P. R. China

[‡]Key Lab of Optoelectronic Materials Chemistry and Physics, Fujian Institute of Research on the Structure of Matter, Chinese Academy of Sciences, Fuzhou 350002, P. R. China

Supporting Information

ABSTRACT: Metal phosphates have been popularly regarded as excellent luminescence hosts of lanthanide ions, while such an issue is challenged by the ignorance about the structural stability that may originate from the different chemical nature between the framework and the dopant lanthanide ions. Here, we choose $BiPO_4$ as a model compound to study. A detailed investigation of the effects of Eu doping and annealing on the structures and related luminescence properties of $Bi_{1-x}PO_4:Eu_x$ (x = 0−0.199) has been carried out. A monoclinic phase (denoted as LTMP) was obtained for the undoped sample, which gradually transformed to a hexagonal phase (HP) with increasing doping level of Eu^{3+} to x = 0.068. Further, it is also found that annealing had an obvious impact on the structures of the resulted samples. With increasing the annealing temperature up to 400 °C a phase transformation from HP to LTMP happens, which is opposite to that with doping. The above phase transformation behaviors were further confirmed by performing structural studies of doping with Dy^{3+} ions and annealing undoped $BiPO_4$. The structural evolution had a great influence on the luminescent properties. Initially a significant decrease in Eu^{3+} luminescence intensity and quantum efficiency was observed when LTMP transformed to HP. Afterward, a converse situation, increasingly enhanced luminescence performance, appeared when HP transformed to LTMP. Therefore, whether metal phosphates could be taken as better luminescence hosts must take into account their structural changes caused by the different chemical natures between framework and dopant ions, which may provide an important reference for designing new luminescent materials.

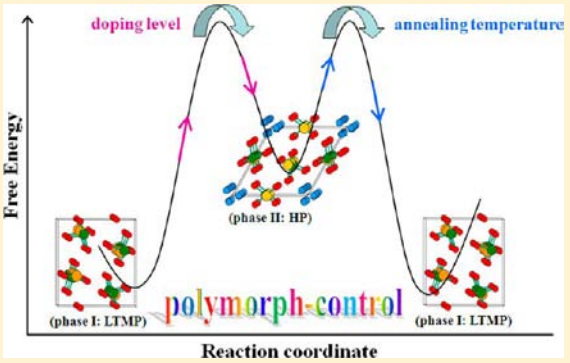

INTRODUCTION

Inorganic luminescent materials have found extensive applications in displays, LEDs, lasers, optoelectronics, and fluorescent markers in biomedicine.[1−3] The majority of these materials are generally obtained by doping luminescent rare-earth ions in hosts. As a result, the chemical nature of the hosts has had a great impact on the properties and moreover applications of inorganic luminescent materials.[4,5] To date, many efforts have been made to design or fabricate hosts for developing high-performance luminescent materials.[6−8] Several excellent hosts have thus been achieved, which include YVO_4,[9−11] $CaWO_4$,[12,13] $Ba_3Ga_3N_5$,[14] $BaHfO_3$,[15] $Sr_3Si_2O_4N_2$,[16] or $NaYF_4$.[17] Despite some major progress, the search for novel hosts still faces challenges, primarily originating from the uncertainties in the structural stabilities of hosts when doping luminescent rare-earth ions.

Motivated by this, $BiPO_4$ was taken as a model host and Eu^{3+} as a dopant to study for the following reasons. (i) It is isostructural to metal phosphates ($M^{3+}PO_4$, M = Y, Ln), which have been widely utilized as hosts for many phosphors.[18,19] (ii) Just like other metal phosphates, $BiPO_4$ may have rich phases like monazite, xenotime, rhabdopane, weinschenkite, or orthorhombic form.[20] One may expect that any tiny structural changes of hosts upon doping can be highly sensitively detected. (iii) Dopant Eu^{3+} and framework Bi^{3+} of hosts have the same oxidation states, while their chemical natures are quite different alike many other phosphors. The structural changes, if any, for host $BiPO_4$ upon doping Eu^{3+} may have more important implications about the structural stabilities of hosts for many phosphors. In particular, (iv) it is still unclear if $BiPO_4$ is a better host for rare-earth luminescent ions. Naidu et al.[21] did not observe any phase transitions of $BiPO_4$ as the dopant level of La^{3+} increases from 0 to 100%. It seems that $BiPO_4$ is a better luminescent host. In fact, La^{3+} is not a luminescent dopant and could not yield any emission among all lanthanide systems, because of the electronic configuration of $4d^{10}$. Comparatively, Eu^{3+} possesses a $4f^6$ configuration, relatively narrow emission band, and long lifetimes of the excited states, which allows it to be a known luminescent ion for red light emission.[22,23] However, previous reports related to Eu^{3+}−$BiPO_4$ are partial, which do not take into account the effect of

Received: September 4, 2012
Published: December 26, 2012

 © 2012 American Chemical Society dx.doi.org/10.1021/ic3019315 | Inorg. Chem. 2013, 52, 807−815

Eu^{3+} on the structural stability of the $BiPO_4$ host. For instance, Zhou et al. did not observe any phase structural change in Li^+ and Eu^{3+}-codoped $BiPO_4$.[24] Recently, we initiated a solvent-driven room-temperature reaction route and prepared $BiPO_4$:Eu^{3+} at a low doping level (<5 mol %). It is found that the structure of the host $BiPO_4$ varies depending on the types of solvent.[25] We also investigated the phase transformation behavior and related luminescence properties of $BiPO_4$:Eu with specific components (doping level of Eu^{3+} ions was maintained at 5 mol %). It is indicated that the structural changes of $BiPO_4$ were closely associated with the reaction temperature.[26] Even so, it is not known if the host $BiPO_4$ could maintain its structure when varying the doping level of Eu^{3+} in a broader range.

Herein, we systematically studied the host structures of $BiPO_4$ and the relevant luminescence properties via doping and annealing. To this purpose, a monoclinic phase (denoted as LTMP) was first prepared without doping. It is demonstrated that this phase structure gradually transformed to a hexagonal phase (HP) with increasing Eu^{3+} concentrations. Surprisingly, such a phase transformation sequence is totally changed upon annealing. Accompanying these transformations, the luminescent properties became very different. The findings reported here are fundamentally important, which may provide a basis for designing new hosts for luminescent materials.

EXPERIMENTAL SECTION

Sample Preparation. All reagents employed in the experiments were analytical grade and used without further purification. Samples $Bi_{1-x}PO_4$:Eu_x (x = 0−0.199) were prepared by hydrothermal reaction of $Bi(NO_3)_3{\cdot}5H_2O$, $Eu(NO_3)_3{\cdot}5H_2O$, and $NH_4H_2PO_4$ in a mixture solution of deionized water and ethylene glycol, which have been described in our previous work with a few modifications.[26,27] Typically, 5 mL of an ethylene glycol solution of 2 mmol of nitrate [$Bi(NO_3)_3{\cdot}5H_2O$ + $Eu(NO_3)_3{\cdot}6H_2O$] with a fixed molar ratio of Eu/Bi and 2 mmol of $NH_4H_2PO_4$ were dissolved in 65 mL of deionized water under constant stirring for 30 min. A white homogeneous suspension was formed, which was transferred to a Teflon-lined stainless autoclave with a capacity of 100 mL. The autoclave was tightly closed and maintained at 180 °C for 12 h. As the autoclave cooled down to room temperature naturally, white precipitates were synthesized, collected by filtration, washed with distilled water several times, and dried at 60 °C for 6 h for further characterization.

In order to see the phase change, the as-prepared sample of $Bi_{0.801}PO_4$:$Eu_{0.199}$ was annealed at different temperatures (e.g., 400, 500, 600, and 700 °C) for 2 h.

Sample Characterization. Chemical analysis of the samples was performed using an inductively coupled plasma (ICP) technique on a Perkin-Elmer Optima 3300DV spectrometer. Powder X-ray diffraction (XRD) patterns of the samples were collected using a Rigaku MiniFlex II apparatus equipped with Cu Kα radiation (λ = 0.15418 nm). Lattice parameters and phase compositions were calculated using a profile fitting by a least-squares method employing the computer program GSAS implemented with EXPGUI[28] in which Ni powders served as an internal standard for peak position calibration (as illustrated in Figure S1, Supporting Information). Thermal gravimetric analysis was carried on a STA449F3 thermal analyzer at a heating rate of 20 K min^{-1} in air over the temperature range of 30−1000 °C. FT-IR spectra of the samples were recorded on a Perkin-Elmer Spectrum One spectrometer in the range of 400−4000 cm^{-1} with a resolution of 4 cm^{-1} using a KBr pellet technique. The molar ratio of the sample to KBr is set at 5‰. Field-emission scanning electron microscopic (FE-SEM) images of the samples were taken by a JEOL JSM-6700 operating at a 10.0 kV beam energy. Electron paramagnetic resonance (EPR) spectra were measured on a Bruker ELEXSYS E300 spectrometer at liquid nitrogen temperature. The spectrometer was operated in the X-band frequencies with a modulation frequency at 100 kHz.

Luminescence Measurement. Photoluminescent spectra of the samples were carried out at room temperature by a Varian Cary Eclipse Fluorescence Spectrometer. Decay time curves were measured by single photocounting with a Vary Eclipse Lifetimes Application setup. For photoluminescence comparison, all measurements were performed under the same conditions (like sample mass, light pass, and so on).

RESULTS

Stoichiometry and XRD Analysis. Elemental analyses of the as-prepared samples were performed using the ICP technique. As indicated in Table 1, the molar ratios of Bi:Eu:P detected for all samples were close to the initial ones. Therefore, the formula for the samples can be thus described as $Bi_{1-x}Eu^{3+}_xPO_4$ (x = 0, 0.010, 0.022, 0.053, 0.068, 0.099, 0.152, 0.199). It means that Eu was successfully incorporated into $BiPO_4$ through hydrothermal reactions.

Table 1. Initial Molar Ratios and Those Experimentally Measured by ICP Technique for the As-Prepared $Bi_{1-x}Eu_xPO_4$ Samples in Hydrothermal Conditions

initial molar ratios Bi:Eu:P	ICP measured ratios Bi:Eu:P	deduced formula of the final product
1:0:1	1.000:0:1.000	$BiPO_4$
0.990:0.010:1	0.990:0.010:1	$Bi_{0.990}Eu_{0.010}PO_4$
0.980:0.020:1	0.978:0.022:1	$Bi_{0.978}Eu_{0.022}PO_4$
0.950:0.050:1	0.947:0.053:1	$Bi_{0.947}Eu_{0.053}PO_4$
0.930:0.070:1	0.932:0.068:1	$Bi_{0.932}Eu_{0.068}PO_4$
0.900:0.100:1	0.901:0.099:1	$Bi_{0.901}Eu_{0.099}PO_4$
0.850:0.150:1	0.848:0.152:1	$Bi_{0.848}Eu_{0.152}PO_4$
0.800:0.200:1	0.801:0.199:1	$Bi_{0.801}Eu_{0.199}PO_4$

To investigate the influence of doping level on the structures of $BiPO_4$, the hydrothermally prepared samples $Bi_{1-x}PO_4$:Eu_x (x = 0−0.199) were examined by XRD. As indicated in Figure 1a, without Eu^{3+} ions added (i.e., x = 0), all diffraction peaks matched well a low-temperature monoclinic phase (LTMP, JCPDS, no. 15-0767), while no other peaks from Eu_2O_3 or impurities can be detected, which indicated a pure LTMP phase. As the doping level of Eu^{3+} ions increased to 0.053, LTMP phase remained. Further increasing the doping level to 0.068 led to a phase transformation from LTMP to HP, as characterized by very weak diffraction peaks (100) and (101) around two theta of 14.7° and 20.2°, respectively. HP became the dominant phase when the doping level further increased. At a doping level of 0.099, the content of the HP component was about 55.0 wt %, as illustrated in Table 2. The phase composition of HP increased with increasing doping level of Eu^{3+} ions. At a doping level of 0.152, the content for the HP component was as high as 98.4 wt %. The very weak diffraction peaks (011) and (−111) around 19.2° and 21.6° indicated the presence of tiny LTMP phase. As the Eu^{3+} ion concentration reached 0.199, all diffraction peaks could be readily indexed to a hexagonal phase (HP, JCPDS, no. 45-1370). All these results demonstrate that the phase structures of $BiPO_4$:Eu can be readily tuned by adjusting the lanthanide doping level.

Lattice variations with lanthanide doping were examined by evaluating the lattice parameters. Unit cell lattice parameters of the as-prepared samples $Bi_{1-x}PO_4$:Eu_x (x = 0−0.199) were obtained using least-squares profile fitting, listed in Table 2 (also see Figure S1, Supporting Information). As presented in

dx.doi.org/10.1021/ic3019315 | Inorg. Chem. 2013, 52, 807−815

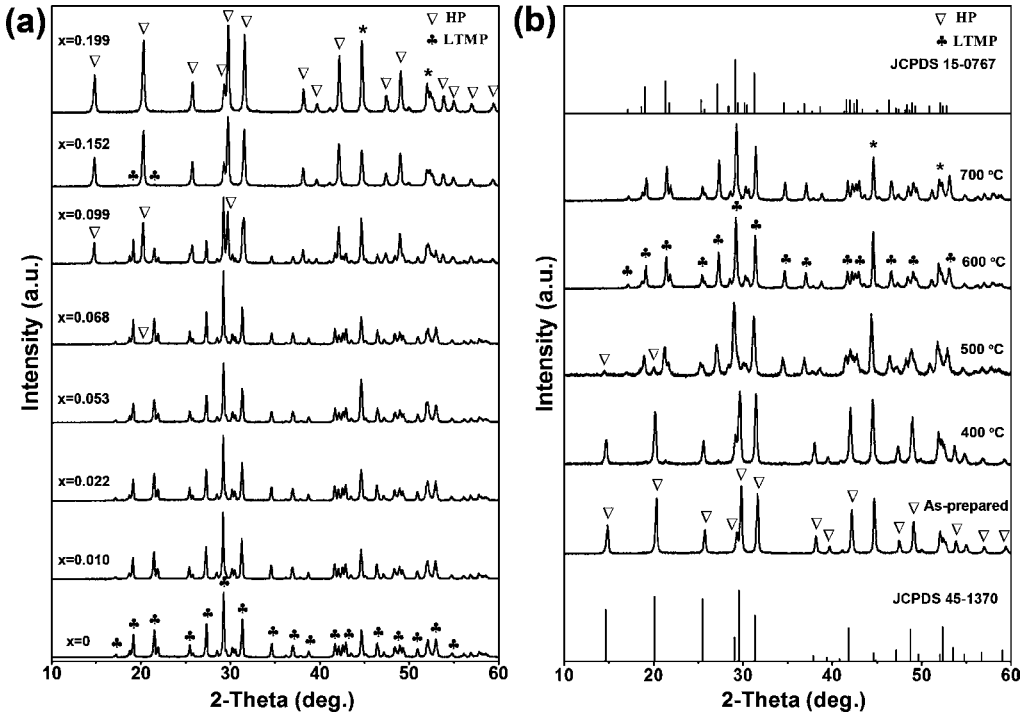

Figure 1. XRD patterns of (a) as-prepared $Bi_{1-x}PO_4:Eu_x$ at given doping levels of Eu and (b) $Bi_{0.801}PO_4:Eu_{0.199}$ after annealing at given temperatures along with JCPDS card nos. 45-1370 (HP) and 15-0767 (LTMP). Asterisk (*) represents the diffraction lines of the internal standard, nickel.

Table 2. Phase and Phase Fraction and Lattice Parameters of the Samples $Bi_{1-x}PO_4:Eu_x$ (x = 0–0.199) Prepared by the Hydrothermal Method and the As-Prepared $Bi_{0.801}PO_4:Eu_{0.199}$ Annealed at Different Temperatures

	phase fraction (%)		cell parameters							
			LTMP phase					HP phase		
sample $Bi_{1-x}PO_4:Eu_x$, x =	LTMP	HP	a (Å)	b (Å)	c (Å)	β	V (Å^3)	a (Å)	c (Å)	V (Å^3)
0	100	0	6.7552(2)	6.9416(2)	6.4781(2)	103.692(2)	295.14(2)			
0.010	100	0	6.7552(2)	6.9423(3)	6.4733(2)	103.697(3)	294.94(2)			
0.022	100	0	6.7502(2)	6.9381(2)	6.4720(2)	103.708(2)	294.48(2)			
0.053	100	0	6.7423(2)	6.9308(2)	6.4638(2)	103.718(3)	293.44(2)			
0.068	99.0	1.0	6.7504(2)	6.9401(3)	6.4707(2)	103.721(3)	294.49(2)	6.942(8)	6.53(2)	272.5(7)
0.099	45.0	55.0	6.7515(3)	6.9398(4)	6.4712(3)	103.713(4)	294.56(3)	6.9583(2)	6.4475(3)	270.35(2)
0.152	1.6	98.4	6.733(2)	6.888(4)	6.526(3)	103.62(4)	294.1(2)	6.9703(2)	6.4589(3)	271.76(2)
0.199	0	100						6.9650(2)	6.4509(3)	271.01(2)
0.199, 400 °C	11.3	88.7	6.731(3)	6.918(4)	6.474(4)	103.68(5)	292.9(2)	6.9679(4)	6.4538(4)	271.36(4)
0.199, 500 °C	89.1	10.9	6.7610(5)	6.9505(5)	6.4683(5)	103.826(7)	295.15(4)	6.985(2)	6.477(3)	273.6(1)
0.199, 600 °C	100	0	6.7430(2)	6.9344(3)	6.4535(2)	103.777(3)	293.08(2)			
0.199, 700 °C	100	0	6.7201(3)	6.9126(3)	6.4336(2)	103.761(3)	290.28(2)			

Table 2, for undoped $BiPO_4$, the refined cell parameters were closer to the standard diffraction data of LTMP (JCPDS, no. 15-0767). As the Eu doping content increased from 0.010 to 0.053, the lattice parameters, a, b, c, and V, of LTMP decreased monotonically. A linear fit to the unit cell volume data (Figure S2, Supporting Information) indicated that the decrease in unit cell volume follows Vegard's law.[29] Since the ionic radius of Eu^{3+} is 1.07 Å, much smaller than that of 1.17 Å for Bi^{3+},[30] this linear decrease in unit cell volume clearly indicates a quantitative substitution of Bi^{3+} by Eu^{3+} in $BiPO_4$ host. For HP phase, the linear decrease in cell volume was also observed as the Eu doping content increased from 0.152 to 0.199 (Figure S2, Supporting Information).

These variations in the structures of $BiPO_4$ host with Eu^{3+} doping appear to be totally different from those reported by Naidu et al.[21] For the latter case, the phase structure of $BiPO_4$ host remains monoclinic as the dopant level of La^{3+} increases from 0 to 100%. Then, they claimed that $BiPO_4$ is a better host for lanthanide doping. Such a conclusion is questionable since it does not consider how the structural stability occurs to the host originated from the different chemical natures between the framework and the dopant ions. In this case, La^{3+} is unsuitable as a representative lanthanide ion dopant to investigate structural changes of $BiPO_4$, since the ionic radius of La^{3+} (1.16 Å) is quite close to that of 1.17 Å for Bi^{3+}.[30] Thus, Naidu et al. did not observe any phase transition though the dopant content is very high (100% substitution). Alternatively, when doping Eu^{3+} at a high level, a phase transformation occurs from LTMP to HP. However, it should be noted that to dope a high content of Eu^{3+} ions into $BiPO_4$ host via hydrothermal

dx.doi.org/10.1021/ic3019315 | Inorg. Chem. 2013, 52, 807–815

reactions one key point needs to be considered: Bi^{3+} and Eu^{3+} salts have different dissolution properties. Impurity phases usually appeared, such as α-Bi_2O_3 in hydrothermal systems.[31] To overcome this problem, we designed a path for Eu^{3+} to be quantitatively incorporated into $BiPO_4$, which includes first dissolution of $Bi(NO_3)\cdot 5H_2O$ and $Eu(NO_3)\cdot 6H_2O$ in a small amount of ethylene glycol (5 mL) and then mixing with $NH_4H_2PO_4$ solution. As ethylene glycol is a weak reducing agent, it might convert part of Eu^{3+} to Eu^{2+} species under hydrothermal conditions. As shown in the EPR spectra (Figure S3, Supporting Information), no characteristic signals of Eu^{2+} ions were present for samples $Bi_{1-x}PO_4:Eu_x$ (x = 0, 0.022, 0.099, 0.199).[32,33] Therefore, the effects of Eu^{2+} ions on the above phase transformation could be ruled out. A series of experiments on the other lanthanide ions like Dy^{3+}, which do not undergo a change in the oxidation state under hydrothermal conditions, was also carried out. As displayed in the XRD patterns (Figure S4, Supporting Information), a phase transformation occurs from LTMP to HP with increasing doping concentrations of Dy^{3+}, which was similar to the phase transformation behavior when Eu^{3+} was chosen as dopant ion.

The structural stability of as-prepared $Bi_{0.801}PO_4:Eu_{0.199}$ was examined through annealing at high temperatures. Figure 1b shows the XRD patterns of the obtained samples along with JCPDS card nos. 45-1370 and 15-0767. It can be clearly seen that HP phase gradually transformed to LTMP with increasing annealing temperature, as shown in Table 2. For instance, the phase fraction of the LTMP component is 11.3% at 400 °C, which increased to 89.1% at 500 °C. Further increasing the annealing temperature to 600 °C led to a pure phase LTMP, as indicated by data comparison to JCPDS card no. 15-0767. Such a reversible phase transformation from HP to LTMP also occurs to $BiPO_4$:Dy annealed at 600 °C, as observed in the XRD study (Figure S4, Supporting Information). To further prove that the obtained monoclinic form was isostructural with that of LTMP obtained by hydrothermal methods, structural studies of undoped $BiPO_4$ and those obtained by annealing undoped $BiPO_4$ at different temperatures were also carried out. As shown in the XRD patterns (Figure S5, Supporting Information), the phase transformation behavior of these samples was similar to the doped samples. Compared with the Bi−O and P−O bond lengths of these samples shown in Table S1, Supporting Information, the monoclinic form obtained at 600 °C is indeed isostructural with that of LTMP obtained at 180 °C through hydrothermal reactions. However, the monoclinic form obtained at 700 °C was another monoclinic modification of $BiPO_4$, i.e., high-temperature monoclinic form (HTMP), which was in accordance with the reported data.[34] The reversible phase transformation from HP to LTMP was further investigated using thermogravimetric analysis (TGA) and differential thermal analysis (DTA). As shown in Figure 2a, $Bi_{0.801}PO_4:Eu_{0.199}$ underwent a continuous mass loss in a wide temperature range from room temperature to 500 °C accompanied by an exothermal peak at 350 °C. This exothermal peak was associated with the phase transformation from HP to LTMP, which was in accordance with the XRD analysis. For undoped $BiPO_4$, there is not any mass weight loss in the detected temperature range (Figure 2b), while the water molecules in some of the lanthanide phosphates could stabilize even at high temperatures. For instance, Luwang et al.[35] reported that water molecules in YPO_4 could stabilize up to 800 °C and a phase transformation from hexagonal phase (hydrated) to tetragonal phase (dehydrated) occurs with

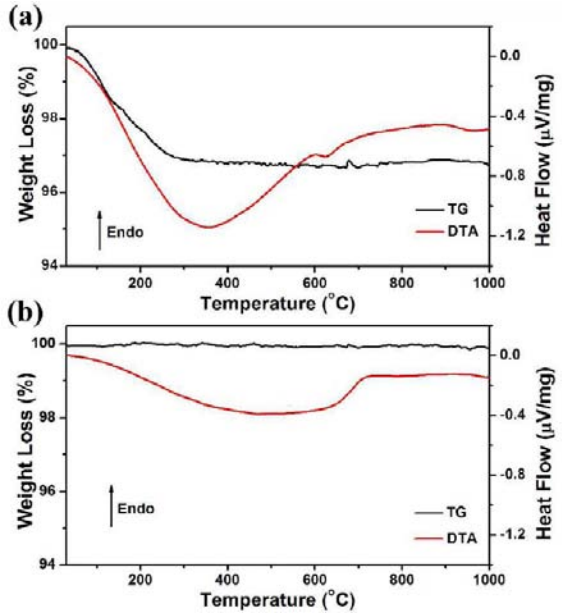

Figure 2. Comparative TGA and DTA curves of (a) $Bi_{0.801}Eu_{0.199}PO_4$ and (b) $BiPO_4$ obtained using hydrothermal methods at 180 °C for 12 h.

further increasing annealing temperature. Zollfrank et al.[36] also reported a phase transformation from hydrated europium orthophosphate ($EuPO_4\cdot nH_2O$) of hexagonal crystal structure to monoclinic dehydrated $EuPO_4$ at 600 °C. From the dehydrated temperature for both phosphates, it is not difficult to see that the binding force of Eu−O (directly coordinated to water molecules, as shown in FT-IR spectrum) is much stronger than that of Bi−O. There are two main reasons for such observations. (i) The ionic property of Eu−O is higher than that of Bi−O due to the lower electronegativity of Eu (1.20) than Bi (2.02). (ii) The bond length of Eu−O is shorter than that of Bi−O. Considering these structural factors, the phase transformation from LTMP to HP with increasing dopant level of Eu^{3+} could also be well illustrated. In addition, the second exothermal peak above 600 °C in the DTA curves of both $Bi_{0.801}PO_4:Eu_{0.199}$ and undoped $BiPO_4$ samples (shown in Figure 2a and 2b) were associated with the phase transformation from LTMP to the high-temperature monoclinic bismuth phosphate form (HTMP).

SEM Study. Variations in morphologies and particle sizes that accompany the phase changes of $BiPO_4$ by doping and annealing were examined. As indicated by the SEM images in Figure 3, for undoped samples, the products were composed of nearly all prism-shaped particles in microscale magnitude, except for some small nanorods (Figure 3a). When the Eu doping content was set at 0.022, either phase structure or prism-shaped morphology was maintained (Figure 3b). With increasing Eu doping level, phase transformation from LTMP to HP occurred, resulting in variation of the morphology from prism-shaped particles to much smaller nanorods. For instance, when the Eu doping content increased to 0.053, the products consisted of a mixture of prism-shaped particles and nanorods. Increasing the doping content to 0.099 led to a pure HP phase with a morphology that is composed of nearly all nanorods with diameters of 30−80 nm and lengths ranging from several nanometers to hundreds of nanometers (Figure 3c). When further increasing the doping content to 0.199, either phase

dx.doi.org/10.1021/ic3019315 | Inorg. Chem. 2013, 52, 807−815

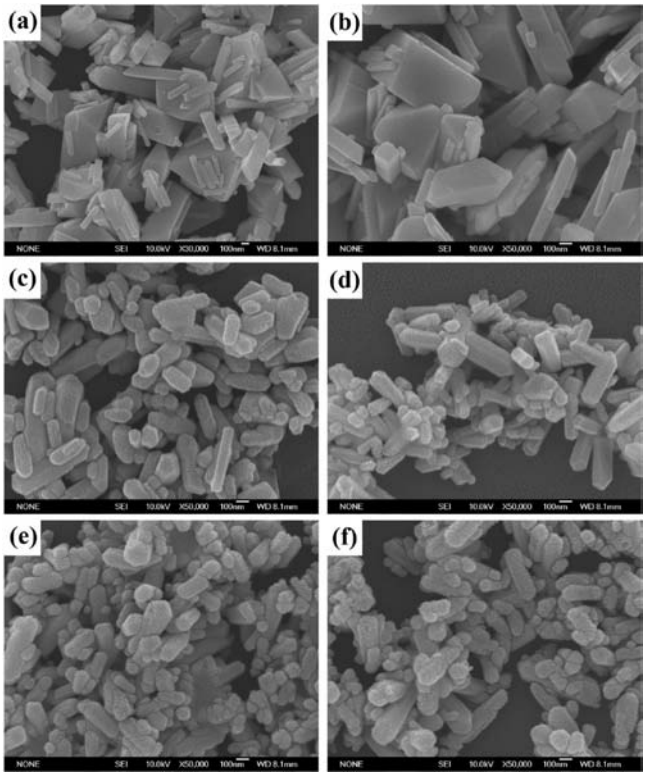

Figure 3. FE-SEM images of the as-prepared samples $Bi_{1-x}PO_4:Eu_x$ with given doping contents of Eu: x = (a) 0, (b) 0.022, (c) 0.099, and (d) 0.199. FE-SEM images of the samples $Bi_{0.801}PO_4:Eu_{0.199}$ after annealing at different temperatures: (e) 400 and (f) 600 °C.

structure or rod-like morphology was maintained, except for the increased aspect ratio of rod-like morphology (Figure 3d). Considering the annealing effects, the morphologies and sizes of the as-prepared samples showed slight changes, as shown in Figure 3e and 3f.

FT-IR Study. The microstructure changes with polymorphs were further investigated by FT-IR spectra. As shown in Figure 4a, there is no absorption band above the wavenumber region of 1500 cm^{-1} for the LTMP phase (x = 0–0.053). Two intense vibration bands in this region became gradually strong in intensity with increasing doping content. For instance, when the Eu doping level x = 0.099, the main absorption band in the region of hydroxyl stretching is centered at 3496 cm^{-1}. According to the literature, this band can be assigned to the stretching vibration, ν(O–H), of the water coordinated directly to the bismuth atoms in the HP phase.[37] The shoulder at 3538 cm^{-1} is probably due to ν(O–H) of the water absorbed on the surface of the sample. Another band associated with hydroxyls is located at 1611 cm^{-1}, which characterizes the vibrations δ(H–O–H).[38] Both stretching and bending vibrations for O–H groups become gradually strengthened in intensity with increasing doping content of Eu^{3+} ions. These variations were consistent with the above structural evolutions from LTMP to HP. However, both stretching and bending vibrations for O–H groups of the annealed samples gradually vanished with increasing annealing temperature, as shown in Figure 4b. This case was associated with another phase transformation from HP to LTMP, as reported in our recent work.[27]

Symmetric changes of PO_4^{3-} tetrahedra with polymorphs were also investigated by FT-IR. As shown in Figure 4a, some distinct differences can be clearly seen in their vibrational characteristics with respect to phosphate groups. On the basis of group-theoretical analysis,[39] the isolated PO_4 group has T_d symmetry with nine internal modes that can be presented as eq 1

$$\Gamma_{vib} = A_1 + E + 2F_2 \quad (1)$$

where the E representation is doubly degenerated and F_2 is triply degenerated. The mode belonging to the A_1 representation and one of the triply degenerated F_2 modes corresponds to the symmetric (ν_1) and asymmetric (ν_3) P–O stretching vibrations of the PO_4 group, respectively, whereas the E mode and the other F_2 mode representation stand for O–P–O bending ν_2 and ν_4, respectively. For isolated PO_4 tetrahedra in aqueous solution, the experimental wavenumber values for ν_1, ν_2, ν_3, and ν_4 are 938, 420, 1017, and 567 cm^{-1}, respectively.[40] Once the phosphate groups are incorporated into the crystal lattice, depending upon the symmetry around the phosphate

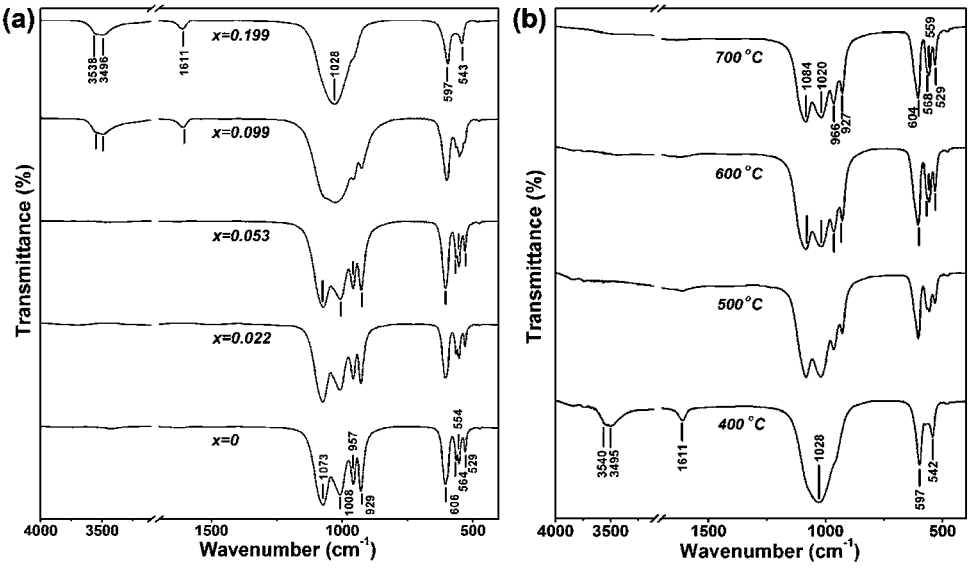

Figure 4. FT-IR spectra of (a) samples $Bi_{1-x}PO_4:Eu_x$ with given doping contents of Eu and (b) $Bi_{0.801}PO_4:Eu_{0.199}$ annealed at different temperatures.

dx.doi.org/10.1021/ic3019315 | Inorg. Chem. 2013, 52, 807–815

group and the nature of the charge balance cation, the above modes undergo either a blue shift or a red shift. For the present work, the PO_4 group in sample $Bi_{1-x}PO_4:Eu_x$ (x = 0–0.053) has a C_1 symmetry, since all four P–O bonds are different, with lengths varying between 1.238 and 1.489 Å (Table S2, Supporting Information). The ν_3 stretching vibration of the PO_4 group was gradually split, characteristic of LTMP. On the basis of previous studies on different phosphates,[41−43] bands at 1073, 1008, and 957 cm^{-1} have been attributed to the ν_3 asymmetric stretching vibration of P–O bonds and that around 929 cm^{-1} is assigned to the corresponding ν_1 symmetric vibration. The bending vibration of O–P–O linkages appeared around 606, 564, 554, and 529 cm^{-1}.[44] With increasing doping content, phase transformation from LTMP to HP occurred, leading to the increased symmetry of the PO_4 group. For instance, the symmetry of the PO_4 groups in the sample at x = 0.199 is further increased to C_2 with two different P–O bond lengths (1.341 and 1.479 Å, Table S2, Supporting Information) and can be considered to have a pseudo-T_d symmetry. Under this symmetry, the ν_3 mode of vibration is triply degenerated, which is so close to the ν_1 mode of vibration that they overlap significantly to give a very intense band centered at 1028 cm^{-1}. The corresponding ν_2 and ν_4 modes appear around 597 and 543 cm^{-1}, respectively.[45] Reversely, the symmetry of the PO_4 groups from pseudo-T_d symmetry to C_1 could also be achieved by annealing the Eu^{3+} doping HP at different temperatures, as shown in Figure 4b, which have also been schematically examined in our recent work.[27]

Luminescence Properties. Figure 5 shows the excitation spectra of the samples $Bi_{1-x}PO_4:Eu_x$ with Eu doping content of

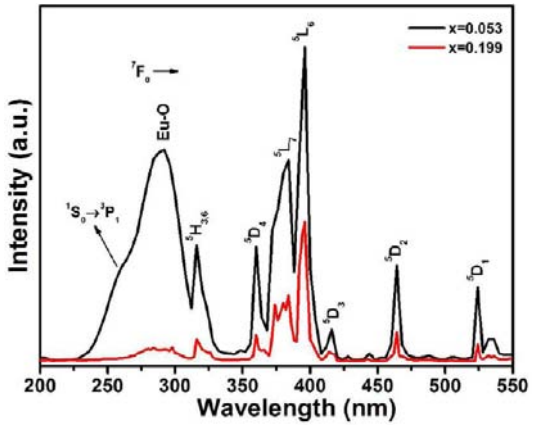

Figure 5. Typical excitation spectra of as-prepared samples $Bi_{1-x}PO_4:Eu_x$ with Eu doping content of x = 0.053 and 0.199.

x = 0.053 and 0.199. PLE spectra were measured by monitoring the emission $^5D_0$–$^7F_1$ (593 nm) at room temperature in the range of 200–550 nm. A 550 nm long-pass emission filter was mounted onto the device to eliminate excitation and scattered light prior to data collection. It is shown that there exists a broad intense band at 290 nm with a shoulder at 260 nm along with many sharp peaks in the wavelength range of 310–550 nm. The broad band centered at 290 nm corresponds to the Eu–O charge-transfer band (CTB), which arose from the transition of the 2p electrons of O^{2-} to the empty 4f orbitals of Eu^{3+} ions.[46] The shoulder at 260 nm, overlapping the intense band, is due to the $^1S_0 \rightarrow {}^3P_1$ transition of Bi^{3+} ions.[47] Several sharp lines were observed in the longer wavelength region, located at 316, 360, 384, 394, 416, 464, and 524 nm, which correspond to the intrinsic transitions from the ground state, $^7F_0$, to the excitation multiplets, $^5H_{3,6}$, $^5D_4$, $^5L_7$, $^5L_6$, $^5D_3$, $^5D_2$, and $^5D_1$ of Eu^{3+} ions.[48] It was also observed that the relative intensity of both the charge-transfer band (CTB) and intrinsic transitions of Eu^{3+} ions decreased with phase transformation from LTMP (x = 0.053) to HP (x = 0.199), which infers that LTMP has a higher energy transfer efficiency when compared to HP (Figure 5).

Figure 6 shows the photoluminescent spectra of the samples $Bi_{1-x}PO_4:Eu_x$ obtained with given dopant contents. Emission

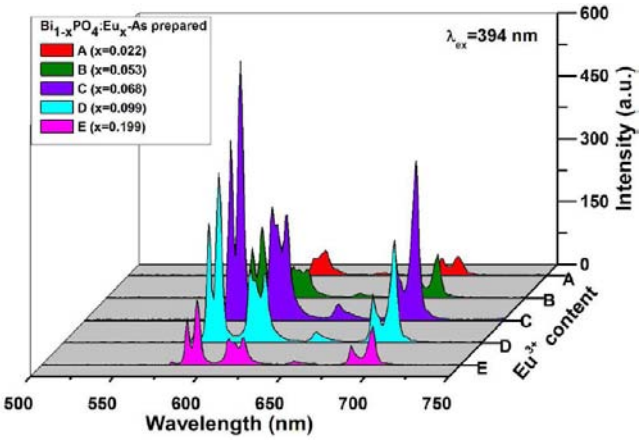

Figure 6. Emission spectra of the samples $Bi_{1-x}PO_4:Eu_x$ with given doping contents of Eu prepared in hydrothermal conditions at 180 °C for 12 h.

spectra were measured at room temperature in the range of 400–850 nm. Upon excitation into the $^7F_0$–$^5L_6$ transition at 394 nm, an orange-red color was observed, characteristic of the transitions $^5D_0$–^7F_J (J = 0, 1, 2, 3, 4) of Eu^{3+} ions. The strong emission bands around 593 and 618 nm are associated with transitions $^5D_0$–$^7F_1$ and $^5D_0$–$^7F_2$, respectively, while bands in the range of 642–670 and 674–714 nm are assigned to transitions $^5D_0$–$^7F_3$ and $^5D_0$–$^7F_4$, respectively.[49] To compare the luminescence intensity, the integrated areas under the magnetic and electric dipole transitions were calculated and are summarized in Table S3, Supporting Information. The relative emission intensity becomes gradually strengthened with increasing dopant content, since an increase in Eu concentration might give rise to more luminescent active sites. The emission intensity reached a maximum when the dopant content was up to x = 0.068. Further, the luminescence of Eu^{3+} decreases suddenly with an increase of the Eu^{3+} dopant concentrations. Above x = 0.152, luminescence intensity is almost constant. There is a slight increase in the luminescence intensity at excess Eu^{3+} doping (x = 0.199), which might be an effect from total formation of hydrated HP (observed in the XRD study).

Figure 7 shows the emission spectra of the as-prepared $Bi_{0.801}PO_4:Eu_{0.199}$ and those products obtained by annealing it at different temperatures. The spectra exhibit a typical emission peak of Eu^{3+} at 593 nm corresponding to the magnetic dipole transition ($^5D_0$–$^7F_1$) along with peaks at 618 and 697 nm assigned to electric dipole transitions ($^5D_0$–$^7F_2$, $^5D_0$–$^7F_4$). Apart from these, a weak emission peak centered at 650 nm ascribed to the $^5D_0$–$^7F_3$ transition is also observed. There is a sudden enhancement of the Eu^{3+} emission peak for 500–700 °C, which was not observed at 400 °C. As stated above in the

dx.doi.org/10.1021/ic3019315 | Inorg. Chem. 2013, 52, 807–815

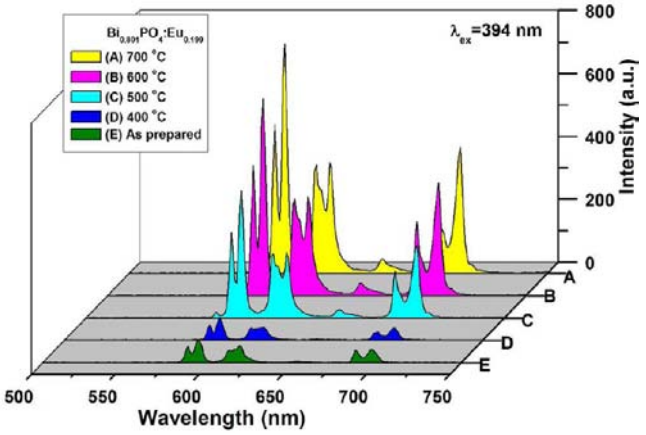

Figure 7. Emission spectra of as-prepared $Bi_{0.801}PO_4:Eu_{0.199}$ and those products obtained after annealing at different temperatures.

XRD studies, there is a phase transformation to dehydrated from hydrated phase as the temperature rises from 500 to 700 °C. It is noted that the recovery of luminescent intensity in the 500−700 °C annealed sample is due to the crystal structure transformation from hydrated to dehydrated phase. Also, these observations clearly demonstrate that the luminescence performance is sensitive to the evolution of the polymorphs of $BiPO_4$.

Figure 8a shows the luminescence decay for the $^5D_0$ level of Eu^{3+} in $Bi_{1-x}PO_4:Eu_x$ (x = 0.053 and 0.199). Excitation and emission wavelengths are fixed at 394 and 593 nm, respectively. To understand the behavior of luminescence decay, we tried fitting (using the Origin 8.0 program) to the decay data. It is found that the curves exhibit a single-exponential feature that can be well reproduced by a monoexponential function as in eq 2

$$I = I_0 \exp(-t/\tau) \tag{2}$$

where I is the intensity at time t, I_0 is the intensity at $t = 0$, and τ is the decay lifetime. Similar decay kinetic behaviors were also observed in other $BiPO_4$ samples. The lifetimes for all $Bi_{1-x}PO_4:Eu_x$ samples are listed in Table 3. With increasing Eu^{3+} dopant concentrations, the lifetime for the $^5D_0$ level of Eu^{3+} decreases from 2.55 to 0.668 ms.

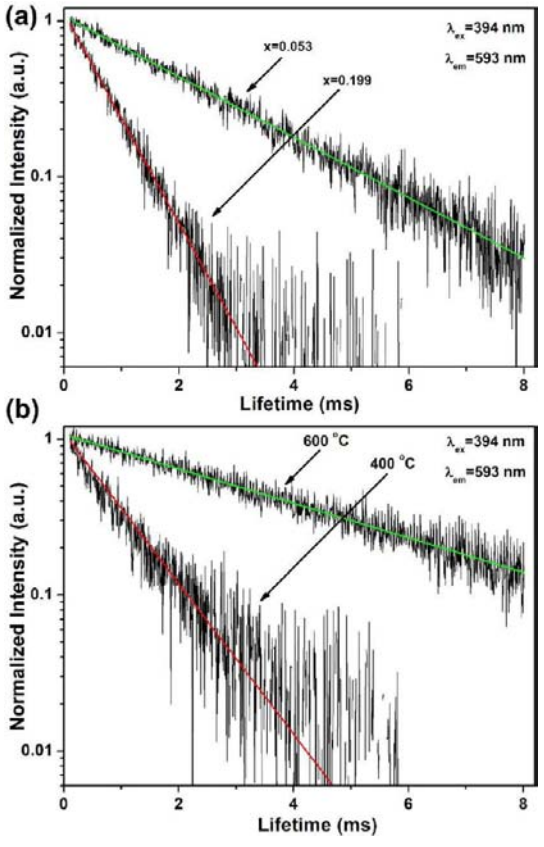

Figure 8. (a) Decay curves for samples $Bi_{1-x}PO_4:Eu_x$ with x = 0.053 and 0.199 prepared by hydrothermal methods; (b) decay curves for those obtained after annealing $Bi_{0.801}PO_4:Eu_{0.199}$ at 400 and 600 °C.

Table 3. Decay Time, Luminescence Quantum Efficiency, η (%), and Nonradiative Part (%) of the Hydrothermally Prepared Samples $Bi_{1-x}PO_4:Eu_x$ (x = 0.010−0.199) and $Bi_{0.801}PO_4:Eu_{0.199}$ Annealed at Different Temperatures

sample $Bi_{1-x}PO_4:Eu_x$, x =	decay time (λ_{ex} = 394 nm)/ms	η (λ_{ex} = 394 nm) (%)	nonradiative part (%)
0.010	2.55	37.10	62.90
0.022	2.45	35.27	64.73
0.053	2.26	32.49	67.51
0.068	2.24	32.22	67.78
0.099	1.43	21.23	78.77
0.152	0.659	10.90	89.10
0.199	0.668	11.08	88.92
0.199, 400 °C	0.90	14.74	85.26
0.199, 500 °C	3.39	71.39	28.61
0.199, 600 °C	3.98	62.56	37.44
0.199, 700 °C	4.00	61.66	38.34

When the $Bi_{0.801}PO_4:Eu_{0.199}$ sample is annealed at different temperatures (Figure 8b), the lifetime value shows little change up to 400 °C. However, the decay time of the 500 °C heated sample, in which the phase transformation occurs, shows a significant enhancement in decay lifetime (Table 3). This sudden increase in decay lifetime is related to the phase transformation from a hydrated HP to a dehydrated LTMP. On further increasing the annealing temperature (600−700 °C), the decay time was nearly maintained, keeping a relative fixed value (3.38 ms). These observations clearly demonstrate that the decay time is also sensitive to the evolution of the polymorphs of $BiPO_4$.

Apart from the luminescent lifetime, another important characteristic is the quantum efficiency of the emitting system. It is defined as the ratio of the number of emitted photons to the number of absorbed photons. It can also be related to the radiative and nonradiative rate constants, assuming that only these processes occur as in eq 3.[50,51]

$$\eta = \frac{k_r}{k_r + k_{nr}} \tag{3}$$

In the case of Eu^{3+}, an approximation allows calculation of the $^5D_0$ quantum efficiency directly from the emission spectrum and the measured luminescence lifetime. Because of the pure magnetic dipole character of the $^5D_0-{}^7F_1$ transition, it can be taken as an internal reference. The radiative rate constant k_r may be calculated from the relative intensities of the $^5D_0-{}^7F_J$ transitions according to eq 4.[52]

dx.doi.org/10.1021/ic3019315 | Inorg. Chem. 2013, 52, 807−815

$$k_r = A_{0-1}\frac{\hbar\omega_{0-1}}{I_{0-1}}\sum_{J=0}^{4}\frac{I_{0-J}}{\hbar\omega_{0-J}} \quad (4)$$

The emission intensities are obtained by deriving the integrated area S under the corresponding lines, where i and j represent the initial ($^5D_0$) and final (F_J) levels. Due to the poor intensity of the $^5D_0-^7F_{5,6}$ transitions, only the remaining $^5D_0-^7F_{0-4}$ transitions were taken into consideration. The barycenters of the observed lines were taken as the transition energy $\hbar\cdot\omega_{0-J}$. In addition, A_{0-1} is Einstein's coefficient of spontaneous emission between the $^5D_0$ and $^7F_1$ levels, which is 50 s^{-1}.[53] In summary, calculation of the integrated areas and barycenters of all $^5D_0-^7F_{0-4}$ transitions lead to the radiative rate constant k_r. With the measured luminescence lifetime, the nonradiative rate constant k_{nr} can be calculated according to eq 5.

$$\tau = (k_r + k_{nr})^{-1} \quad (5)$$

Finally, the $^5D_0$ quantum efficiency is determined by adding the obtained values of k_r and k_{nr} to eq 3. It has to be noted that the $^5D_0$ quantum efficiency only concerns emission from the $^5D_0$ level. To consider also emission from higher levels and thus determine the overall quantum efficiency, more complicated and time-consuming methods have to be applied.[54]

The lifetimes and $^5D_0$ quantum efficiencies for $Bi_{1-x}PO_4:Eu_x$ (x = 0.010−0.199) and 400, 500, 600, and 700 °C annealed samples of x = 0.199 are compiled in Table 3. As shown in Table 3, it is clear that the quantum efficiency underwent a continuous decrease with increasing Eu^{3+} doping concentration, exhibiting the variation trend similar to the lifetime (Figure 8a). There was a slow decrease from 37.10% at x = 0.010 to 32.22% at x = 0.068. Strikingly, as LTMP transformed into HP when the doping concentration increased up to 0.099, the quantum efficiency significantly decreased to 21.23%, which further sharply declined to a maximum of 10.90% with an Eu^{3+}content x = 0.152. Increasing the Eu^{3+} doping concentration further, the quantum efficiency was nearly unchanged, only 11.08% for the sample of x = 0.199.

The quantum efficiency of $Bi_{0.801}PO_4:Eu_{0.199}$ was slightly increased when annealed at 400 °C. When the $Bi_{0.801}PO_4:Eu_{0.199}$ sample is annealed at higher temperature, the quantum efficiency of Eu^{3+} shows a sharp increase at 500 °C, which is due to the loss of water molecules on conversion to the dehydrated LTMP phase from hydrated HP phase. On further increasing the annealing temperature (600−700 °C), the quantum efficiency is almost constant.

As presented above, phase transformation and evolution processes have been schematically controlled by doping and annealing, which could have a great effect on the energy transfer process and electronic structure and thus the luminescence performance. To understand the variations of luminescence properties of different polymorphs of $BiPO_4$:Eu, several structural factors, such as the local symmetry environment of Eu^{3+}, the symmetry for the lattice site of Eu^{3+} in both polymorphs follows the sequence LTMP < HP, which has been demonstrated by the variations in structural symmetry. Hence, the luminescence performance for $BiPO_4$:Eu is expected to decrease with the symmetric enhancement, as previously reported for $LaPO_4$:Eu of different polymorphs.[55] This expectation is in accordance with what we observed in $BiPO_4$ polymorphs. Another important factor could be from the lattice water: its impact on the luminescence properties gradually becomes significant as LTMP transforms to HP. In particular, hydration for HP has shown a quenching effect on the luminescence.

With regard to the dipole moment, considering their structure and structural parameters (Figure S6 and Tables S2 and S4, Supporting Information), the dipole moment of polymorphs could be estimated according to eq 6

$$\vec{\mu} = q\vec{r} \quad (6)$$

where $\vec{r}$ is the displacement vector pointing from the negative charge to the positive charge.

The values of the dipole moment in Bi(Eu)−O polyhedra are 1.569 and 0.733 D for LTMP and HP, respectively. The larger dipole moment for LTMP means that the dopant Eu^{3+} resides at sites more deviated from the centers of positive and negative charges. Meanwhile, the LTMP phase possesses stronger emission intensity and a longer decay time, which indicates that the dipole moment may be responsible for the variation trends of luminescence performance for Eu^{3+} in these polymorphs. Given all these structural factors, the LTMP phase has shown a superior luminescence performance to HP. Considering our recent work,[25−27] $BiPO_4$ as a better luminescent host should meet the following conditions: a lower dopant concentration (≤5 mol %) and proper annealing temperature (400 °C ≤ annealing temp. ≤ 600 °C).

CONCLUSION

In the present work, $BiPO_4$ as the host of Eu^{3+} ions was examined by monitoring the structures and relevant luminescence properties under doping and annealing. Systematic evaluation of the sample characterization indicated that the doping level and annealing temperature had a great impact on the structural stability and related luminescence properties of $Bi_{1-x}PO_4:Eu_x$ (x = 0−0.199). For the undoped sample, it possessed a LTMP structure, which gradually transformed to HP with increasing Eu^{3+} concentration. Moreover, the annealing temperature also had an obvious impact on the structures of the resulting products. The reversible phase transformation from HP to LTMP happens with increasing annealing temperature. These phase transformation behaviors were further demonstrated by implementing the structural investigation of doping with Dy^{3+} ions and annealing undoped $BiPO_4$. The structure evolution had a great influence on the luminescent properties, also clearly indicated by the changes in decay time, quantum efficiency, and nonradiative transition, in which several structural factors, such as the symmetry environment of Eu^{3+}, lattice water, and dipole moment of Bi(Eu)−O polyhedra, have been well considered. Therefore, whether metal phosphates could be taken as better luminescence hosts, one must take into account their structural changes caused by the different chemical natures between framework and dopant ions.

ASSOCIATED CONTENT

Supporting Information

Rietveld refinements; variation of cell volume; EPR spectra; XRD patterns; crystal structures of HP and LTMP; lattice parameters, atomic positions, and bond lengths. This material is available free of charge via the Internet at http://pubs.acs.org.

dx.doi.org/10.1021/ic3019315 | Inorg. Chem. 2013, 52, 807−815

AUTHOR INFORMATION

Corresponding Author

*E-mail: guangshe@fjirsm.ac.cn.

Notes

The authors declare no competing financial interest.

ACKNOWLEDGMENTS

This work was financially supported by NSFC (Nos. 21025104, 51072198, 50972143, 91022018) and the National Basic Research Program of China (2011CBA00501).

REFERENCES

(1) Wang, F.; Tan, W. B.; Zhang, Y.; Fan, X. P.; Wang, M. Q. *Nanotechnology* **2006**, *17*, R1−R13.
(2) Ishow, E.; Brosseau, A.; Clavier, G.; Nakatani, K.; Tauc, P.; Fiorini-Debuisschert, C.; Neveu, S.; Sandre, O.; Leaustic, A. *Chem. Mater.* **2008**, *20*, 6597−6599.
(3) Wang, W. X.; Yang, P. P.; Cheng, Z. Y.; Hou, Z. Y.; Li, C. X.; Lin, J. *ACS Appl. Mater. Interfaces* **2011**, *3*, 3921−3928.
(4) Feldmann, C.; Justel, T.; Ronda, C. R.; Schmidt, P. J. *Adv. Funct. Mater.* **2003**, *13*, 511−516.
(5) Su, Y. G.; Li, L. P.; Li, G. S. *Chem. Mater.* **2008**, *20*, 6060−6067.
(6) Wang, F.; Han, Y.; Lim, C. S.; Lu, Y.; Wang, J.; Xu, J.; Chen, H.; Zhang, C.; Hong, M.; Liu, X. *Nature* **2010**, *463*, 1061−1065.
(7) Lorbeer, C.; Cybinska, J.; Mudring, A.-V. *Cryst. Growth Des.* **2011**, *11*, 1040−1048.
(8) Danielson, E.; Golden, J. H.; McFarland, E. W.; Reaves, C. M.; Weinberg, W. H.; Wu, X. D. *Nature* **1997**, *389*, 944−948.
(9) Huignard, A.; Gacoin, T.; Boilot, J. P. *Chem. Mater.* **2000**, *12*, 1090−1094.
(10) Zhao, M.; Li, G.; Zheng, J.; Li, L.; Yang, L. *CrystEngComm* **2012**, *14*, 2062−2070.
(11) Yu, M.; Lin, J.; Wang, Z.; Fu, J.; Wang, S.; Zhang, H. J.; Han, Y. C. *Chem. Mater.* **2002**, *14*, 2224−2231.
(12) Su, Y. G.; Li, L. P.; Li, G. S. *J. Mater. Chem.* **2009**, *19*, 2316−2322.
(13) Lou, Z. D.; Cocivera, M. *Mater. Res. Bull.* **2002**, *37*, 1573−1582.
(14) Hintze, F.; Hummel, F.; Schmidt, P. J.; Wiechert, D.; Schnick, W. *Chem. Mater.* **2012**, *24*, 402−407.
(15) Drag-Jarzabek, A.; Kosinska, M.; John, L.; Jerzykiewicz, L. B.; Sobota, P. *Chem. Mater.* **2011**, *23*, 4212−4219.
(16) Wang, X. M.; Wang, C. H.; Kuang, X. J.; Zou, R. Q.; Wang, Y. X.; Jing, X. P. *Inorg. Chem.* **2012**, *51*, 3540−3547.
(17) Mai, H. X.; Zhang, Y. W.; Si, R.; Yan, Z. G.; Sun, L. D.; You, L. P.; Yan, C. H. *J. Am. Chem. Soc.* **2006**, *128*, 6426−6436.
(18) Clavier, N.; Podor, R.; Dacheux, N. *J. Eur. Ceram. Soc.* **2011**, *31*, 941−976.
(19) Tang, C. C.; Bando, Y.; Golberg, D.; Ma, R. Z. *Angew. Chem., Int. Edit.* **2005**, *44*, 576−579.
(20) Yan, R. X.; Sun, X. M.; Wang, X.; Peng, Q.; Li, Y. D. *Chem.—Eur. J.* **2005**, *11*, 2183−2195.
(21) Naidu, B. S.; Vishwanadh, B.; Sudarsan, V.; Vatsa, R. K. *Dalton Trans.* **2012**, *41*, 3194−3203.
(22) Li, H.; Zhu, G.; Ren, H.; Li, Y.; Hewitt, I. J.; Qiu, S. *Eur. J. Inorg. Chem.* **2008**, 2033−2037.
(23) Wiglusz, R. J.; Bednarkiewicz, A.; Strek, W. *Inorg. Chem.* **2012**, *51*, 1180−1186.
(24) Zhou, X.; Wang, X. *Lumines* **2012**, DOI: 10.1002/bio.2416.
(25) Fu, C.; Li, G.; Zhao, M.; Yang, L.; Zheng, J.; Li, L. *Inorg. Chem.* **2012**, *51*, 5869−5880.
(26) Zhao, M.; Li, G.; Li, L.; Yang, L.; Zheng, J. *Cryst. Growth Des.* **2012**, *12*, 3983−3991.
(27) Zhao, M.; Li, G.; Zheng, J.; Li, L.; Wang, H.; Yang, L. *CrystEngComm* **2011**, *13*, 6251−6257.
(28) Toby, B. H. *J. Appl. Crystallogr.* **2001**, *34*, 210−213.
(29) Denton, A. R.; Ashcroft, N. W. *Phys. Rev. A* **1991**, *43*, 3161−3164.
(30) Shannon, R. D. *Acta Crystallogr., Sect. A* **1976**, *32*, 751−767.
(31) Huang, L.; Li, G.; Yan, T.; Zheng, J.; Li, L. *New J. Chem.* **2011**, *35*, 197−203.
(32) Patel, D. K.; Rajeswari, B.; Sudarsan, V.; Vatsa, R. K.; Kadam, R. M.; Kulshreshtha, S. K. *Dalton Trans.* **2012**, *41*, 12023−12030.
(33) Patel, D. K.; Sengupta, A.; Vishwanadh, B.; Sudarsan, V.; Vatsa, R. K.; Kadam, R.; Kulshreshtha, S. K. *Eur. J. Inorg. Chem.* **2012**, 1609−1619.
(34) Mooney-Slater, R. C. L. *Z. Kristallogr.* **1962**, *117*, 371−385.
(35) Luwang, M. N.; Ningthoujam, R. S.; Srivastava, S. K.; Vatsa, R. K. *J. Am. Chem. Soc.* **2011**, *133*, 2998−3004.
(36) Zollfrank, C.; Scheel, H.; Brungs, S.; Greil, P. *Cryst. Growth Des.* **2008**, *8*, 766−770.
(37) Romero, B.; Bruque, S.; Aranda, M. A. G.; Iglesias, J. E. *Inorg. Chem.* **1994**, *33*, 1869−1874.
(38) Li, G. S.; Li, L. P.; Boerio-Goates, J.; Woodfield, B. F. *J. Am. Chem. Soc.* **2005**, *127*, 8659−8666.
(39) Poloznikova, M. E.; Fomichev, V. V. *Usp. Khim.* **1994**, *63*, 419−430.
(40) Pawlig, O.; Schellenschlager, V.; Lutz, H. D.; Trettin, R. *Spectrochim. Acta, Part A: Mol. Biomol. Spectrosc.* **2001**, *57*, 581−590.
(41) Nakamoto, K. *Infrared and Raman Spectra of Inorganic and Coordination Compounds, Part A*; John Wiley and Sons: New York, 1986.
(42) Xue, F.; Li, H. B.; Zhu, Y. C.; Xiong, S. L.; Zhang, X. W.; Wang, T. T.; Liang, X.; Qian, Y. T. *J. Solid State Chem.* **2009**, *182*, 1396−1400.
(43) Arunkumar, P.; Jayajothi, C.; Jeyakumar, D.; Lakshminarasimhan, N. *RSC Adv.* **2012**, *2*, 1477−1485.
(44) Geng, J.; Hou, W. H.; Lv, Y. N.; Zhu, J. J.; Chen, H. Y. *Inorg. Chem.* **2005**, *44*, 8503−8509.
(45) Assaaoudi, H.; Ennaciri, A.; Rulmont, A. *Vib. Spectrosc.* **2001**, *25*, 81−90.
(46) Li, L. P.; Zhao, M. L.; Tong, W. M.; Guan, X. F.; Li, G. S.; Yang, L. S. *Nanotechnology* **2010**, *21*, 195601.
(47) Wolfert, A.; Oomen, E. W. J. L.; Blasse, G. *J. Solid State Chem.* **1985**, *59*, 280−290.
(48) Carnall, W. T. C. H.; Crosswhite, H. M. *Energy level structure and transition probabilities in the spectra of the trivalent lanthanides in* LaF_3; Argonne National Laboratory: Argone, IL, 1978.
(49) Li, L. P.; Su, Y. G.; Li, G. S. *J. Mater. Chem.* **2010**, *20*, 459−465.
(50) Carlos, L. D.; Ferreira, R. A. S.; Bermudez, V. d. Z.; Ribeiro, S. J. L. *Adv. Mater.* **2009**, *21*, 509−534.
(51) Peng, C. Y.; Zhang, H. J.; Yu, J. B.; Meng, Q. G.; Fu, L. S.; Li, H. R.; Sun, L. N.; Guo, X. M. *J. Phys. Chem. B* **2005**, *109*, 15278−15287.
(52) Lima, P. P.; Ferreira, R. A. S.; Freire, R. O.; Paz, F. A. A.; Fu, L. S.; Alves, S.; Carlos, L. D.; Malta, O. L. *ChemPhysChem* **2006**, *7*, 735−746.
(53) Sun, J.; Xian, J.; Xia, Z.; Du, H. *J. Lumin.* **2010**, *130*, 1818−1824.
(54) Wrighton, M. S.; Ginley, D. S.; Morse, D. L. *J. Phys. Chem.* **1974**, *78*, 2229−2233.
(55) Ghosh, P.; Kar, A.; Patra, A. *J. Appl. Phys.* **2010**, *108*, 113506.